Steady Bi-dimensional Crossflow Plasma Jets in Turbulent Channel Flows

(Article begins on next page)

03 September 2025

Steady bi-dimensional crossflow plasma jets in turbulent channel flows

Jacopo Serpieri[1,2*], Marc T. Hehner[1] and Jochen Kriegseis[1]

[1*]Institute of Fluid Mechanics, Karlsruhe Institute of Technology, Kaiserstr. 10, Karlsruhe, 76131, Germany.
[2]Department of Mechanical and Aerospace Engineering, Politecnico di Torino, Corso Duca degli Abruzzi 24, Turin, 10129, Italy.

*Corresponding author(s). E-mail(s): Jacopo.Serpieri@me.com;
Contributing authors: Marc.Hehner@kit.edu;
Jochen.Kriegseis@kit.edu;

Abstract

In this study, the possibility of reducing the friction drag exerted by turbulent flows by means of wall-mounted plasma actuators is experimentally investigated. Two large plasma actuators (PAs) arrays were operated in a channel-flow facility. They were conceived to replicate, the flow control approach investigated by Mahfoze & Laizet ["Skin-friction drag reduction in a channel flow with streamwise-aligned plasma actuator," Int. J. Heat Fluid Flow **66**, 83-94 (2017)] by means of numerical simulations. Namely, steady and relatively largely spaced (378 wall units) actuators were lain down such to induce stationary crossflow-directed fluid motions. Different actuation parameters (actuators' configurations and supplied voltages) and flow Reynolds numbers were tested. Flow static pressure measurements were performed along with the actuators mechanical and electrical characterization. The resulting values of drag manipulation and actuation efficiency are reported. The tested flow actuation led to overall higher values of flow friction drag, whereas values overcoming the value of 30 % of drag reduction were measured at the more downstream actuation positions.The discrepancy with the above reference is deemed to be mainly due to the finite flow actuation hereby considered. Nevertheless, a slightly different Reynolds number was here considered while the actuators effect was measured to be considerably weaker.

Keywords: Active flow control, Drag reduction, Plasma actuators

1 Background and motivation

For conventional airborne vehicles, friction drag represents the most significant share in the drag budget, accounting for nearly 50 % during cruise. As such, efforts aiming at reducing it attracted the interest of major research centers and industry. Thorough reviews on the topic can be found in [1] and [2]. Along with passive techniques mainly based on miniaturized surface patterns (e.g. ridges, riblets or superhydrophobic coatings) and blowing/suction of the boundary layer through permeable walls, oscillating the flow-exposed walls along the crossflow/spanwise direction induces a secondary Stokes flow, which proved to hamper the turbulence generation mechanisms thus leading to reduced skin friction drag [3]. Accordingly, several studies were carried out showing very large values (> 30%) of friction drag reduction. These were based on both numerical (e.g [4–6]) and experimental (e.g. [7–11]) approaches, where the latter had to engineer rather complicated mechanisms and facilities.

With the aim of achieving similar effects while simplifying the actuation embodiment, electric-effect and electromagnetic-effect actuators were considered and deployed too. To the first category take part the plasma actuators (PAs) whether of the AC dielectric barrier discharge (DBD) type (see e.g. [12–15]) or of the pulsed DC corona discharge type (e.g. [16]); to the second, the Lorentz-force based actuators (see e.g. [17, 18]). These efforts also reported very large values of drag reduction.

By means of numerical simulations, Mahfoze & Laizet [19] investigated several flow control strategies of a turbulent channel flow actuated by DBD PAs - or, better, by phenomenological models of their effect -. One considered actuators relatively largely spaced (378 wall units), compared to the [12, 13] actuators, along the crossflow direction and constantly blowing along one crossflow direction. This actuation strategy achieved up to 33% of drag reduction compared to the naturally-occurring flow. These results appear very interesting as this approach would further simplify the flow actuation setup while, at the same time, reduce the consumed power, thus improving both the technological implementation and the actuation efficiency. Nonetheless, experimental validations are needed as the simulations of Mahfoze and Laizet [19] exploit periodic boundary conditions along both the crossflow and the streamwise direction. This approach is fully legitimate and justified by the characteristics of fully-developed channel flows. Moreover, it much reduces the computational cost of highly-resolved simulations and, as such, has been adopted in most of the dedicated numerical-based literature [1–3]. Yet, in real-world applications, the finite size of the flow actuators needs to be accounted for, as it can lead to important findings. This effect has been investigated by Quadrio & Ricco [20] who investigated the transient phase of the oscillating wall actuation in a turbulent channel flow, by Skote [21], Quadrio [22], and Choi et al. [23] who also studied the oscillating wall transients but for boundary layer flows and by Whalley & Choi [12] who also investigated a boundary layer flow but forced by PAs. Investigating the spatial transient effects from PA actuation of turbulent streams was also one main object of the research by Zong et al. [24].
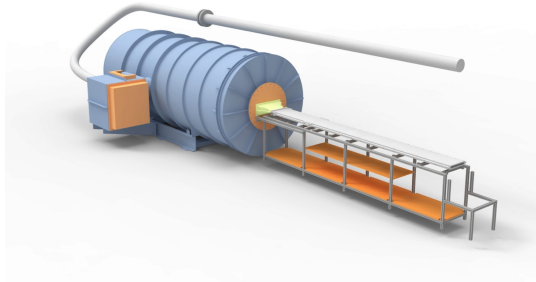
Fig. 1 CAD rendering of the channel-flow facility installed at the ISTM.

Straub et al. [25] studied instead the effect of the finite extension along the spanwise/crossflow direction of oscillating wall actuation.

The objective of the research described in this document is twofold. Firstly, it aims at the experimental validation of the steady crossflow-unidirectional and largely spaced actuation proposed by Mahfoze & Laizet [19]. To do so, it experimentally investigates a turbulent channel flow actuated by two very large (12.5 m of total plasma discharge each) DBD PAs operated at different voltages on flows at different Reynolds numbers. The first-time application and operation of such large DBD PA arrays in experiments is the second (hands-on proof of concept) objective of the present investigation.

2 Experimental setup

2.1 Flow facility and diagnostics

The channel-flow facility where the current research was performed is installed at the Institute of Fluid Mechanics (ISTM) laboratory (cp. [9, 26–28]). The facility is characterized as a blower wind tunnel. The air flowing through the tunnel is not circulated, leading to better heat dissipation and higher robustness of the flow parameters. It has permanently-assembled sidewalls that are in near-perfect alignment, with exchangeable top and bottom plates. The full length of the test section is 3950 mm, consisting, for the considered cases, of ≈ 950 mm of flow development area and ≈ 3000 mm of the actual measurement area. The test section is rectangular with 300 mm in width W and 25.2 mm in height H. A schematic of the facility can be seen in Figure 1. As shown in the schematics, the air is accelerated by a fan installed in the cubic chamber placed at the side of the cylindrical settling chamber. The inlet of the air flow of the fan chamber is the pipe that goes around the settling chamber. In this pipe, an orifice flange is installed to measure the inlet flow rate (refer to [9, 26–28] for details). On the test section side, at the inlet of the channel, a flow tripping device was installed on both the upper and lower wall to force the flow transition to the turbulent state. 21 pressure taps pairs consisting of 0.3 mm holes drilled on the channel side walls at the symmetry plane allowed

to retrieve the static pressure distribution along the channel. Each of the taps making a pair were connected together before the transducer, thus retrieving a single, averaged measurement. The taps pairs are spaced 200 mm apart in the streamwise direction and, thus, span 1.9 m of the test section length. The pressure taps are connected to a high-precision pressure transducer (*MKS Baratron 698A*) featuring an accuracy of $\pm 0.05\%$ of its full scale (100 Torr). This is a differential pressure transducer and the ambient pressure is used as reference. The measurements were performed at friction Reynolds numbers (Re_τ) ranging between $250 \leq Re_\tau \leq 405$.

The streamwise direction is indicated with x, the wall-normal one with y and the crossflow one with z. These are shown in the schematic of figure 3. Accordingly, the velocity components along these directions are referred to as u, v and w, respectively.

2.2 Flow actuators

2.2.1 Layout

The DBD PAs in this study used 0.5 mm thick polyethylene terephthalate (PET) sheets as dielectric layer. The electrodes were made with 0.35 mm thick - 5 mm wide copper tape and the isolation of the encapsulated electrodes was guaranteed by multiple layers of *Kapton* tape. The exposed electrodes were supplied with a high voltage (HV) signal and the encapsulated ones were connected to the ground. To ensure there is no undesired plasma formation between the electrodes and the wind-tunnel metallic structure, and to avoid influencing the static-pressure measurements, a distance of 20 mm from the tunnel sidewalls was left clear of electrodes. This results in arrays of plasma actuators (APAs) spanning 290 mm in width and 675 mm in length each. A photography of one array installed and operated in the channel-flow facility is shown in figure 2. Two APAs were fabricated and were conceived to generate a series of jets aligned along the z direction similarly to the numerical setup of Mahfoze & Laizet [19]. A schematic of the APAs installed in the channel-flow facility is shown in figure 3. The actuators of the array were spaced at a distance of $D = 15.12$ mm along the crossflow direction (see figure 3). This value leads to a spacing of $D^+ = 378$ wall units for a flow at $Re_\tau = 315$ in the
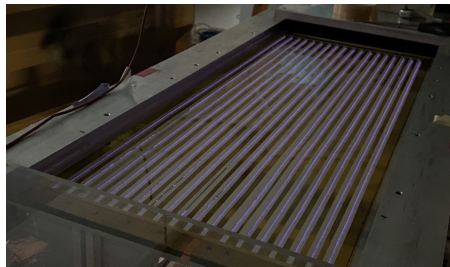

Fig. 2 Photography of one APA installed and operated in the channel-flow facility with the upper wall removed. The plasma discharges glow in light black.
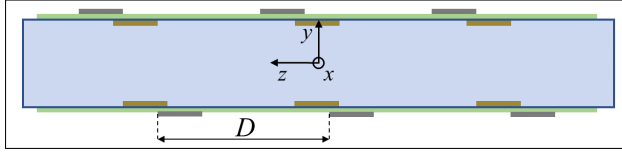
Fig. 3 Schematic (not to scale) of the two APAs installed in the channel-flow facility (*parallel* configuration) as seen from downstream, and definition of the reference system and of the actuators' spacing D. The actuators' dielectric layer is shown in light green, the exposed electrodes in yellow and the encapsulated ones in gray.

considered channel flow facility. This spacing, for the case of steady unidirectional actuation, was found by Mahfoze & Laizet [19] to lead to the highest value of drag reduction (33 %). Each APA is made of 18 actuators spanning the whole channel in width, therefore, considering the extension of 0.675 m in the streamwise direction, a total length of 12.5 m of plasma discharge per APA was attained.

The APAs were mounted in two configurations. One, *parallel* configuration, featured them one mounted on the upper and one on the lower wall of the tunnel, at the same streamwise station, and blowing in opposite crossflow directions (indicated in figure 3). The other, *series* configuration, instead, considered both of them mounted on the upper wall, one after the other in the streamwise direction and both blowing along the same crossflow direction.

The power supply used in this experiment is a *HP 6269B*, which can deliver up to 40 V and 50 A. This was used to power two, one per APA, high-voltage (HV) transformers: *Minipuls 6* by *GBS Elektronik GmbH*. The amplitude of the power supply output signal was adjusted such to lead to a peak-to peak voltage V_{pp} on the APAs electrodes equal to 7, 8 and 9 kV. An *Agilent Technology DSOX2004A* oscilloscope was used to generate a sinusoidal signal oscillating at the frequency of $f_{AC} = 4$ kHz fed as input to the HV suppliers.

An overview of the tested parameters and configurations is reported in table 1.

Table 1 Tested flow and actuation parameters.

V_{pp} [kV]	Re_τ	configuration	jets direction APA1 | APA2
0, 7, 8, 9	250, 360, 405	*parallel*	$+z$ | $-z$
0, 7, 8, 9	250, 360, 405	*series*	$+z$ | $+z$

2.2.2 Mechanical characterization

The flow fields induced by the actuators operated at the mentioned voltages and frequency were measured apart by means of a PIV experiment, where the actuators were characterized in quiescent flow. To do so, they were installed and operated in an $\approx 1\,\mathrm{m}^3$ perspex box seeded with $\approx 1\,\mu\mathrm{m}$ DEHS particles.
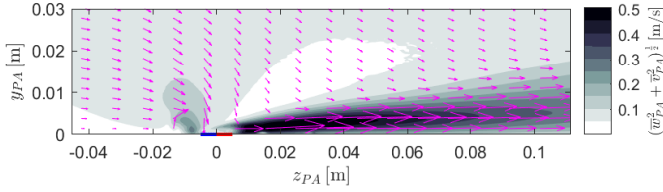
Fig. 4 Time-averaged velocity field induced by a single, isolated, 2D PA operated at $V_{pp} = 9\,$kV in quiescent flow. The exposed and encapsulated electrodes are shown with blue and red lines, respectively. One every 12 measured vectors is shown for clarity.

Particles illumination was achieved with a *Litron Nano L200-15 PIV* laser (200 mJ/pulse) and images were captured with an *Andor Zyla* sCMOS camera (5.5 Mpx and 16 bits of resolution). The system was operated at 15 Hz and 200 image pairs per case were acquired. These were processed with a spline-based interpolation [29], multi-pass algorithm with image deformation and correlation windows' weighting functions [30, 31] to retrieve velocity fields. The optical resolution and processing parameters are such to retrieve one vector every 0.20 mm along the wall-normal direction.

The time-averaged velocity field induced by a single, isolated, 2D PA (whose quantities are denoted with an overbar and the PA subscript) operated at $V_{pp} = 9\,$kV in quiescent flow is shown in figure 4. From this velocity field and from the ones acquired for the different operated voltages, the maximum induced velocity $max(\overline{w}_{PA})$ was extracted. Moreover, considering the momentum balance within a control volume which is far enough from the actuator to neglect pressure variations [32], the induced thrust T_{PA} was computed. These quantities are reported in table 2 together with the maximum induced velocity non-dimensionalized with the friction velocity of the flow at the different considered friction Reynolds numbers $max(\overline{w}_{PA}^+|_{Re_\tau})$ for all the operated voltages. All these quantities are related to the main effect induced by PAs: a

Table 2 Time-averaged PA-induced thrust $\overline{T}_{PA}$ along z and y, maximum $\overline{w}_{PA}$ and minimum $\overline{v}_{PA}$ values of velocity in dimensional units and non-dimensionalized with the tested flows' friction velocity (denoted with the $+$ superscript) for the different supplied peak-to-peak voltages.

V_{pp} [kV]	$\overline{T}_{PA}^z$ [mN/m]	$max(\overline{w}_{PA})$ [m/s]	$max(\overline{w}_{PA}^+)$ $Re_\tau = 250$	$max(\overline{w}_{PA}^+)$ $Re_\tau = 360$	$max(\overline{w}_{PA}^+)$ $Re_\tau = 405$
7	0.16	0.29	1.35	0.93	0.84
8	0.50	0.44	1.76	1.21	1.09
9	1.05	0.54	1.80	1.24	1.12
V_{pp} [kV]	$\overline{T}_{PA}^y$ [μN/m]	$min(\overline{v}_{PA})$ [m/s]	$min(\overline{v}_{PA}^+)$ $Re_\tau = 250$	$min(\overline{v}_{PA}^+)$ $Re_\tau = 360$	$min(\overline{v}_{PA}^+)$ $Re_\tau = 405$
7	-2.39	-0.21	-0.67	-0.46	-0.42
8	-22.50	-0.24	-0.77	-0.53	-0.48
9	-41.05	-0.27	-0.86	-0.59	-0.53

mainly wall-aligned jet occurring near the wall and along the direction that goes from the exposed electrode to the encapsulated one, as clearly shown in figure 4. Yet, the continuity of mass requires a mass supply for this wall jet. This causes a suction of mass from the surrounding of the actuator and mainly from the regions upstream of - with respect to the wall jet - the electrodes and above them, also visible in figure 4. While this fluid motion from upstream contributes to induced thrust along the wall-parallel direction, the one from above the electrodes induces a wall-normal flow velocity and thrust directed towards the wall. This secondary effect is deemed very relevant for the considered application as it will be commented upon in the remainder. Thus the minimum value of the induced wall-normal velocity and the wall-normal thrust, respectively referred to as $min(\overline{v}_{PA})$ and $\overline{T}^{y}_{PA}$, were evaluated too from the measured flow fields. They are also reported in table 2.

The non-dimensional induced crossflow velocities hereby reported are considerably lower than the ones considered in Ref. [19] and likewise in most of the oscillating-wall literature ($max(w^{+} = 10)$) [1, 2].

2.2.3 Electric characterization

Electric measurements were also performed to assess the values of the electric power P_E consumed by the actuators arrays for the different voltages here considered. To do so, the mentioned oscilloscope was used also to measure the voltages and the charges on the two APAs by means of two HV probes in series between the HV suppliers and the exposed electrodes and of two $C_p = 100\,\text{nF}$ capacitors in series between the encapsulated electrodes and the ground, respectively. These signals allow to assess the time-averaged power consumed by the actuators arrays [32, 33] by considering equation:

$$P_E = \frac{1}{N} \sum_{i=1}^{N} f_{AC} \oint_T Q(t)\mathrm{d}V(t) = \frac{1}{N} \sum_{i=1}^{N} f_{AC} C_p \oint_T V_p(t)\mathrm{d}V(t), \qquad (1)$$

where Q is the charge crossing the PAs, V_p is the voltage across the capacitor and $T = 1/f_{AC}$ is the period of the AC cycle. The oscilloscope sampling was set to $5.00\,\text{MSa/s}$ and the measurement time was such to acquire $N = 400$ plasma-discharge cycles each of which measured with 1250 samples. The N power-per-cycle measurements were then averaged together to retrieve the APA averaged consumed power as shown in equation 1.

The computed values of the electric power consumed by one APA for the different supplied voltages are reported in table 3 together with the consumed power per length of plasma discharge, where the total plasma discharge length per APA was $l_p = 12.5\,\text{m}$, as well as with the consumed power per actuation length l_a. This last quantity considers the two arrays' configurations, where the consumed power per actuation length for the *parallel* case is twice the one of the *series* configuration. In other terms, the actuation unit length for the *parallel* case l_a^p is half the one for the *series* configuration l_a^s.

The averaged consumed power was measured for all the different tested cases. Small differences were reported with varying the operated flow speed. Nevertheless, it is not easy to discern whether these were due to the interactions with the incoming flow or to the actuators' wear-out process. Besides, the variation of DBD PAs' performance due to prolonged operation is a topic of research on its own (e.g.[34–36]). The P_E values reported in table 3 are, therefore, the averaged values through the measurements at the different flow velocities.

Table 3 Electric power P_E and electric power per length of plasma discharge P_E/l_p and per actuation length P_E/l_a consumed by one APA for the different supplied peak-to-peak voltages.

V_{pp} [kV]	P_E [W]	P_E/l_p [W/m]	P_E/l_a^p [W/m]	P_E/l_a^s [W/m]
7	56.83	4.55	168.39	84.19
8	95.38	7.63	282.61	141.30
9	151.31	12.10	448.33	224.16

3 Results and discussion

3.1 Drag manipulation

Similarly to the approach followed in [9, 26–28], the pressure gradient along the streamwise direction is used to evaluate the wall shear stress coefficient c_f for the different tested flows. This approach is based on

$$c_f = \frac{\tau_w}{0.5\rho V_b^2} = -\frac{\mathrm{d}p}{\mathrm{d}x}\frac{\delta}{0.5\rho V_b^2}, \tag{2}$$

where $\mathrm{d}p/\mathrm{d}x$ is the pressure gradient along the streamwise direction, τ_w is the wall shear stress, δ is the channel half height and V_b is the flow bulk velocity. This last quantity was retrieved by measuring the mass flow rate considering the pressure difference through an orifice plate installed in the pipe supplying air to the tunnel fan (see the schematics of figure 1 and refer to [9, 26–28] for details). The skin friction coefficients of the reference, unforced flows c_{f0} for the tested bulk Re_b and friction Reynolds numbers are reported in the table below.

Table 4 Reference flow skin friction coefficient for the tested Reynolds number flows.

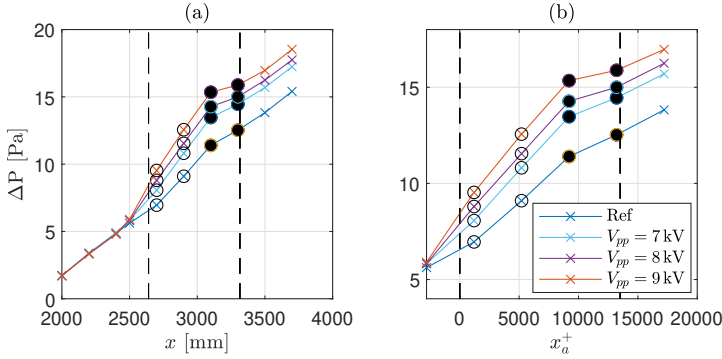| Re_b	Re_τ	c_{f0}
$0.81\,10^4$	250	0.0079
$1.23\,10^4$	360	0.0069
$1.40\,10^4$	405	0.0064

Fig. 5 a: Differential pressure, with respect to the pressure at an upstream station, along the x direction for the different tested flows at $Re_\tau = 250$. APAs in parallel configuration. The x markers indicate the position of the pressure tap pairs and the ○ markers the ones at the APAs. Up/down -stream APAs edges shown with black dashed lines. b: Detail of the ΔP values at the APAs and along the x_a^+ axis.

The differential static pressure along the streamwise direction $\Delta P(x) = p_{ref} - p(x)$, where p_{ref} is the static pressure at a pressure taps pair upstream of the station where the APAs are mounted, was measured for all the tested cases. This is shown in figure 5a, for the reference unforced flow at $Re_\tau = 250$ and for the flow cases, where the APAs were operated in parallel configuration. Figure 5b shows instead a detail considering only the ΔP values pertaining to the pressure taps at the APAs and versus the non-dimensional streamwise direction x_a^+. This latter originates at the most upstream edge of the APAs and is made non-dimensional with the inner-layer length scale for the considered flow ($l^+_{Re_\tau=250} = 49.98\,\mu\text{m}$).

It can be seen that – for the cases where the APAs were operated – the ΔP curves kink upwards at the upstream region of the APAs. Furthermore, this effect is found to be more evident for the higher supplied voltages. In other words, the APAs cause a stronger pressure drop to the oncoming flow. Vice versa, towards the APAs downstream region, the ΔP curves kink downwards (see the filled ○ markers of figure 5). Again, this effect is stronger for the higher voltage cases. In this case, drag reduction takes place as it will be commented upon later. Eventually, downstream of the actuators, the slope of all curves becomes comparable. A small up/downwards kink can be observed also for the reference flow, where no actuation was operated, around the taps placed at $x = 2700\,\text{mm}$. Nonetheless, this case still had the APAs mounted in the test section, which feature some level of roughness/in-homogeneity. This is why, in the remainder, the actuated flow metrics are evaluated with respect to the respective reference flow with the APAs installed and not operated.

The static pressure gradient along the streamwise direction was computed with centered finite differences (with the exception of the first and last point where single-sided differences are considered) and used to evaluate the flow skin friction coefficient. The latter was used to evaluate the effects of the performed flow actuation for the different tested cases. The relative manipulated drag
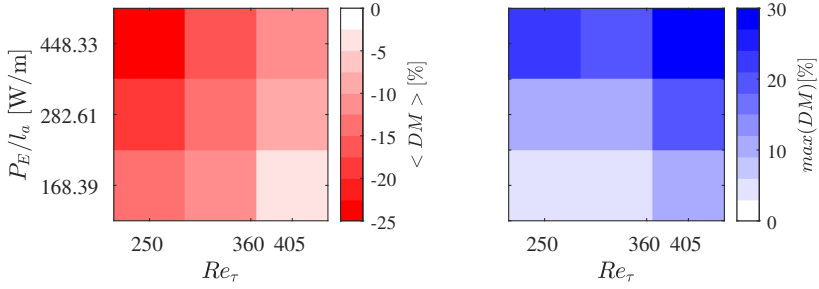
Fig. 6 Maps of streamwise-averaged $< DM >$ (left) and of local maximum $max(DM)$ (right) for the different test conditions with the actuators installed in parallel. See eq. (3) for DM.

DM can be evaluated following the expression in equation (3) between the skin friction coefficient of the reference natural flow c_{f0} and the ones for the forced flows at the same mass flow rate, i.e.

$$DM[\%] = 100\frac{c_{f0} - c_{fa}}{c_{f0}} = 100\frac{\Delta c_f}{c_{f0}}. \tag{3}$$

This procedure was followed for all the measured points. It showed that, at the flow stations near the upstream edge of the actuator, the flow drag was much enhanced by the operated forcing, as already commented upon in the discussion of figure 5. Nonetheless, some considerations should be done here. In fact, estimating the friction drag from the streamwise pressure gradient retrieves correct results only for stationary, fully-developed channel flows. In the performed experiments, the flow features these characteristics only until the upstream edge of the APAs.

Besides the sudden crossflow-directed flow motion close to the wall directly induced by the APAs, a secondary flow motion towards the wall and over the exposed electrodes takes place as described and quantified, for an isolated actuator operated in quiescent flow, in section 2.2.2. This secondary effect causes higher streamwise-momentum fluid particles to approach the channel walls thus locally increasing the friction drag and pressure drop. As shown in figure 5 for the $Re_\tau = 250$ flow, towards the downstream edge of the actuators the slope of the $\Delta P(x)$ curves reduces to then finally recover to the unforced flow value more downstream. This is more evident for the flow cases where the APAs are operated at higher voltages, thus showing a region of drag reduction due to do applied actuation. This region, considering the spatial resolution of the current experiment, extends between $3100\,\text{mm} \le x_a^+ \le 3300\,\text{mm}$ ($9.20\,10^3 \le x_a^+ \le 13.51\,10^3$ for the $Re_\tau = 250$ flow) and is shown with black filled markers in figure 5. It is referred to the extension of this region with the symbol l_a^{DR} throughout the work.

In their study on the oscillating wall transient effects, Quadrio & Ricco [20] report spatial transients of 2000-4000 wall units, for the wall moving at a maximum speed of 6 times the friction velocity ($max(w_w^+ = 6)$) and of 6000-12000 wall units for $max(w_w^+ = 18)$. Choi et al. [23] report a spatial transient
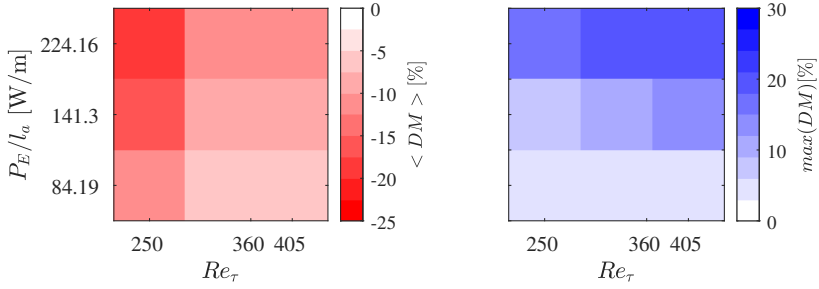
Fig. 7 Maps of streamwise-averaged $< DM >$ (left) and of local maximum $max(DM)$ (right) for the different test conditions with the actuators installed in series. See eq. (3) for DM.

extension of about 5 times the boundary layer thickness in their experiments on an oscillating-plate forced boundary layer flow. Nevertheless, it must be pointed out that a boundary layer flow much differs from a channel flow as it has more possibility to adapt itself to the actuation effect. The considered channel has a height of 25.2 mm and, as seen in figure 4, the actuators' induced downwash extends even to larger wall-normal distances from the wall. The effects of this on the spatial evolution of the actuated flow need to be investigated with flow velocimetry techniques and cannot be addressed in the current study, but the large scale of the APAs hereby considered led to the finding of a strong spatial evolution from the considered flow actuation. Furthermore, as shown in table 2, the PA here considered induce a maximum crossflow velocity of $max(\overline{w}_{PA}^+ \approx 1)$ and reaching the overall maximum value of 1.80 among all the tested cases. Also in this, the considered actuation is quite different compared to the oscillating-wall case, where $max(w_{wall}^+ \approx 10)$ was achieved. This also contributes to the transient effect discrepancy between the mentioned literature and the current findings. Finally, note that the research of Mahfoze & Laizet [19], which mainly inspired this study, is based upon a numerical simulation exploiting periodic boundary conditions in both streamwise and crossflow directions on a steady channel flow. As such, the transient effect of the performed actuation was not addressed in that work.

To account for the effect of the streamwise development of the actuated flow, two different metrics of DM have been considered; namely, the streamwise-averaged $< DM >$ and the local maximum $max(DM)$ measured values. The first quantity estimates the overall actuation effect while averaging the mentioned flow-development effect due to the sudden actuation. In other words, for the $< DM >$ metrics, dp/dx is evaluated as a linear fit through all the measured stations on the APAs and shown with ∘ markers in figure 5. As previously discussed, positive values of drag manipulation occur near the downstream edge of the actuators, where the benefits of the actuation become visible. Therefore for $max(DM)$, the pressure gradient is evaluated only between the taps at $x = 3100$ mm and $x = 3300$ and shown with filled markers in figure 5. These two metrics are computed for all the tested cases

and shown in figure 6 for the APAs' parallel configuration, and in figure 7 for the series configuration.

The values of the streamwise-averaged DM are always negative and arrive to overcome the value of -25 % for the arrays in parallel configuration and operated at maximum power on the $Re_\tau = 250$ flow. This means that the performed actuation always increased the overall friction drag of the operated flow compared to the unforced case. For both APA configurations, the $Re_\tau = 250$ flow shows the overall larger increase of friction drag. This can be due to the fact that, for this lower velocity flow, the mentioned downwash effect, is relatively stronger. Oppositely, the case showing the mildest negative overall effect is the weakest forcing at $Re_\tau = 405$.

The maximum DM maps instead always feature positive values. For the *parallel* configuration, a value overcoming 30 % is measured for the $Re_\tau = 405$ flow actuated at maximum power. The fact that the largest $max(DM)$ occurs for the largest tested Reynolds number flow was not expected as the actuators' spacing was deemed to be optimal for a $Re_\tau = 315$ flow [19]. Nevertheless, the actuator spacing is only one actuation parameter that affects the actuation performance. Another one is the value of the maximum induced velocity scaled with the operated flow friction velocity (see table 2). Yet, also here the performed actuation would suggest that for higher Reynolds numbers, the relative induced velocity becomes weaker and so it could be expected to do the actuation effect. Nevertheless, the flow actuation hereby considered entails much more convoluted flow phenomena, which are unfortunately not discernible here. These need to be further quantitatively inspected to draw clear conclusions and this too will be the goal of future research efforts. Eventually, also for this metrics and for all Re_τ and APAs' configurations, larger actuation powers lead to stronger (beneficial, in this case) effects.

The scenario that takes place when the *series* configuration is considered, shown in figure 7, much resembles the one previously discussed for the *parallel* configuration. Overall, as can be expected, the actuation effect in this case is weaker as the two actuators are placed one after the other along the streamwise direction. Accordingly, the values of both $< DM >$ and $max(DM)$ are milder.

3.2 Actuation efficiency

Combining the consumed power and the pressure measurements together, the actuation efficiency η can be estimated. Nevertheless, as considering the whole actuated channel would lead to overall negative values of drag modification, the actuation efficiency is defined as

$$\eta = \frac{GP^{DR}/l_a}{KP_E/l_a} = \frac{G0.5\rho V_b^3 2W\Delta c_f^{DR}}{KP_E/l_a}, \tag{4}$$

where the superscript DR in the equation denotes values acquired at streamwise positions of the channel section where drag reduction i.e. a positive value of DM is achieved. This flow section is indicated by the black filled markers
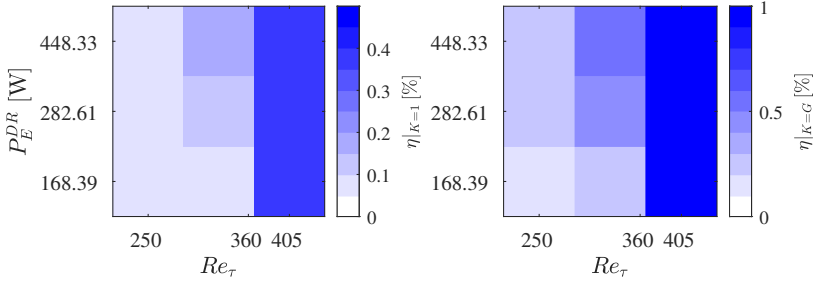
Fig. 8 Maps of actuation efficiency $\eta|_{K=1}$ (left) and $\eta|_{K=G}$ (right) for the different test conditions with the actuators installed in parallel. See eq. (4) for the definition of η.

in figure 5. The drag-manipulation power P_{DM} per actuation length at the numerator considers the flow bulk dynamic pressure multiplied with the bulk velocity, the width of the two channel walls $2\,W$ and the differential skin friction coefficient Δc_f. This last quantity was already introduced in equation (3). Nevertheless, to consider that the saved power only accounts for a small portion (l_a^{DR}) of the overall actuated region (l_a), the numerator presents also the scaling factor $G = l_a^{DR}/l_a$. The input power at the denominator is instead the electric power P_E per actuation length reported in table 3. This is weighted with the coefficient K, whose considered values are 1 and G. When $K = 1$, the whole consumed power per actuation length is considered. This is a penalizing scenario, which takes into account for the overall power per actuation length, including the upstream $DM < 0$ region too. When instead $K = G$ is considered, the electrical power is scaled to account for the APAs portion effectively contributing to the positive drag modification. This considers the best case scenario, where the APAs extend enough that the $DM > 0$ region overcomes the upstream transient part. The efficiency computed following these two approaches and related values of the K coefficient are referred to as $\eta|_{K=1}$ and $\eta|_{K=G}$, respectively.

The outcomes of this analysis are shown in figure 8 for the *parallel* configuration and in figure 9 for the *series* configuration. The efficiency of DBD PAs is known to be rather low [37]. In this case, the actuators are even installed such to induce flow motions orthogonal to the main flow direction. As such, the computed efficiency is expected to attain to very small values. For all the input powers, the evaluated efficiency tends to larger values with increasing Re_τ, as the reported efficiency scales with the flow bulk velocity to the 3rd power. Notwithstanding the chosen metrics, the overall highest value of efficiency is reported for the $Re_\tau = 405$ flow actuated at maximum power for the APAs in series configuration. Despite the larger values of DM reported for the *parallel* forcing, the consumed power per actuation length is half for the *series* configuration and this overcomes the reduced fluid dynamic power gain. Despite the relatively low values and the previous considerations on PAs' efficiency, it should be pointed out that the reported efficiencies compare rather well with previous efforts based on similar or different actuation strategies towards the same goal of reducing friction drag from a turbulent wall-bounded flow. For
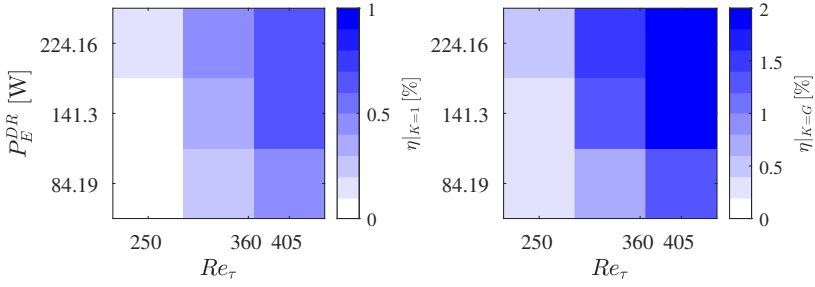
Fig. 9 Maps of actuation efficiency $\eta|_{K=1}$ (left) and $\eta|_{K=G}$ (right) for the different test conditions with the actuators installed in series. See eq. (4) for the definition of η.

example, Auteri et al. [10] reports 0.001 % for their pipe flow investigations; Breuer et al. [18] used Lorentz-force actuation and reported an efficiency of 0.01 %; the same 0.01 % was reported by Jukes et al. [13] for their DBD APA setup, while Gatti et al. [9] reports a value of 0.1 % for their oscillating plate experiments. Finally, the values reported by Thomas et al. [16], are much higher. Nevertheless, the flow actuator that was considered in Ref. [16] works on pulsed DC voltage, whose working principle is very different from the DBD PAs hereby considered and, as such, could be considered a better plasma-based flow actuator to actively reduce skin friction drag.

4 Concluding remarks

The study described in this document aimed at performing a proof-of-concept study of large-scale plasma-actuator operation in experimental AFC investigations, while in turn, experimentally validating the numerical results of [19], where crossflow directed plasma jets are introduced in a turbulent channel flow to reduce the flow friction drag. These results showed very high levels of drag reduction when the flow actuation considered steady and relatively largely spaced actuators along the crossflow direction. This configuration – compared to the ones previously considered in Refs. [13, 14, 38] and aimed at reproducing a flow actuation similar to the Stokes' flow induced by oscillating walls – appears as very attractive for a different reason: In fact, distancing the PAs within the array farther away reduces the possible fluid dynamic (see [24]) or electric (e.g. [39]) interference between narrowly spaced actuators, while it also reduces the power expenditure thus increasing the control efficiency. This becomes more relevant for the application on higher Reynolds number flows that feature reduced spatio-temporal flow scales and, consequently, demand reduced actuators' dimensions.

Two large ($\approx 12.5\,\mathrm{m}$ of plasma discharge each) arrays of DBD plasma actuators were designed, fabricated, installed and operated in a channel flow facility equipped with accurate pressure measurement equipment. The actuation parameters were accordingly scaled, considered the experimental facility, from those of the simulation by Mahfoze & Laizet [19]. Two different configurations were tested considering the actuators arrays either mounted at the

same streamwise position and blowing along opposite crossflow directions, or at subsequent positions and blowing parallel to each other. Different forcing amplitudes and flow Reynolds number were considered. The actuators were both mechanically and electrically characterized in ad hoc setups.

The main outcome from the experimental campaign is that the performed actuation, for all the arrays' configurations, forcing amplitudes and flow Reynolds numbers leads to overall drag enhancement. Nevertheless, local values overcoming 30 % of drag reduction were measured at the more downstream locations. The cause of this streamwise variation and discrepancy from the Mahfoze & Laizet [19] results is deemed to be the streamwise development of the actuation effects, which was not present in the numerical setup of Ref. [19], where periodic boundary conditions also along the streamwise direction were instead considered. Besides this, it should be recalled that the Reynolds number considered in Ref. [19] was smaller ($Re_\tau = 180$) and the actuator model could induce a stronger flow ($max(w^+ = 10)$) compared to the experiments hereby discussed. Finally, the wall-normal extension was also investigated in Ref. [19], showing considerable effect on the operated flow. This could not be varied in our experiments. All these aspects, can further increase the different reported outcomes. Quantitative flow-velocimetry measurement, at different streamwise position, should be carried out to shed light on the underlying flow phenomena and will, accordingly, be the object of future research efforts.

Finally, from the electric measurements of the arrays' consumed power, actuation efficiency maps for all the considered cases were reported too. The efficiency of the considered actuation is, as expected [37], relatively low suggesting that the performed actuation is still to be deemed as at a low TRL. Nevertheless, this study contributes to the TRL advancement, showing the feasibility of manufacturing, operating and testing large arrays of plasma actuators to actively condition the friction drag from turbulent flows. This poses several technological challenges as implies higher power consumption, deployment of large high voltage sources and related EMC issues. Yet, large scale tests are deemed crucial as the streamwise extension of the operated actuation revealed to be a key parameter. While the simplest flow forcing was hereby considered: namely, two-dimensional steady actuators blowing along one crossflow direction (similarly to [16, 19]), more complex flow actuation strategies can be attempted in future aiming at reproducing the flow forcing by oscillating walls (e.g. [6, 7, 9, 23]) or by streamwise traveling waves (e.g. [5, 10, 40]) but induced by plasma actuators arrays (e.g. [12, 14, 16, 38]). Eventually, the maximum measured efficiency, considering the local maximum value of drag reduction, has encouraging values compared with similar goal experimental efforts from literature (e.g. [9, 10, 13, 18]) and could be potentially increased with larger APAs where the drag increasing region at the upstream part of the actuator can have a smaller weight with respect to the drag reduction region on the efficiency budget.

References

[1] Kim, J.: Physics and control of wall turbulence for drag reduction. Philosophical Transactions of the Royal Society A: Mathematical, Physical and Engineering Sciences **369**, 1396–1411 (2011). https://doi.org/10.1098/rsta.2010.0360

[2] Ghaemi, S.: Passive and active control of turbulent flows. Physics of Fluids **32**(8) (2020). https://doi.org/10.1063/5.0022548

[3] Karniadakis, G.E., Choi, K.-S.: Mechanisms on transverse motions in turbulent wall flows. Annual Review of Fluid Mechanics **35**, 45–62 (2003). https://doi.org/10.1146/annurev.fluid.35.101101.161213

[4] Skote, M.: Turbulent boundary layer flow subject to streamwise oscillation of spanwise wall-velocity. Physics of Fluids **23**(8) (2011). https://doi.org/10.1063/1.3626028

[5] Gatti, D., Quadrio, M.: Reynolds-number dependence of turbulent skin-friction drag reduction induced by spanwise forcing. Journal of Fluid Mechanics **802**, 553–582 (2016). https://doi.org/10.1017/jfm.2016.485

[6] Leschziner, M.A.: Friction-Drag Reduction by Transverse Wall Motion - A Review. Journal of Mechanics **36**(5), 649–663 (2020). https://doi.org/10.1017/jmech.2020.31

[7] Choi, K.-S., Graham, M.: Drag reduction of turbulent pipe flows by circular-wall oscillation. Physics of Fluids **10**(1), 7–9 (1998). https://doi.org/10.1063/1.869538

[8] Ricco, P., Wu, S.: On the effects of lateral wall oscillations on a turbulent boundary layer. Experimental Thermal and Fluid Science **29**(1), 41–52 (2004). https://doi.org/10.1016/j.expthermflusci.2004.01.010

[9] Gatti, D., Güttler, A., Frohnapfel, B., Tropea, C.: Experimental assessment of spanwise-oscillating dielectric electroactive surfaces for turbulent drag reduction in an air channel flow. Experiments in Fluids **56**(5), 110 (2015). https://doi.org/10.1007/s00348-015-1983-x

[10] Auteri, F., Baron, A., Belan, M., Campanardi, G., Quadrio, M.: Experimental assessment of drag reduction by traveling waves in a turbulent pipe flow. Physics of Fluids **22**(11) (2010). https://doi.org/10.1063/1.3491203

[11] Marusic, I., Chandran, D., Rouhi, A., Fu, M.K., Wine, D., Holloway, B., Chung, D., Smits, A.J.: An energy-efficient pathway to turbulent drag reduction. Nature Communications **12**(1), 1–8 (2021). https://doi.org/10.1038/s41467-021-26128-8

[12] Whalley, R.D., Choi, K.S.: Turbulent boundary-layer control with plasma spanwise travelling waves. Experiments in Fluids **55**(8) (2014). https://doi.org/10.1007/S00348-014-1796-3

[13] Jukes, T.N., Choi, K.-S.-, Johnson, G.A., Scott, S.J.: Turbulent drag reduction by surface plasma through spanwise flow oscillation. Collection of Technical Papers - 3rd AIAA Flow Control Conference **3**, 1687–1700 (2006). https://doi.org/10.2514/6.2006-3693

[14] Hehner, M.T., Gatti, D., Kriegseis, J.: Stokes-layer formation under absence of moving parts - A novel oscillatory plasma actuator design for turbulent drag reduction. Physics of Fluids **31**(5), 1–6 (2019). https://doi.org/10.1063/1.5094388

[15] Serpieri, J., Hehner, M.T., Pasch, S., Gatti, D., Kriegseis, J.: Introducing a multi-modal plasma actuator for turbulent flow actuation. AIAA Journal, (2023, published online). https://doi.org/10.2514/1.J062812

[16] Thomas, F.O., Corke, T.C., Duong, A., Midya, S., Yates, K.: Turbulent drag reduction using pulsed-DC plasma actuation. Journal of Physics D: Applied Physics **52**(43) (2019). https://doi.org/10.1088/1361-6463/

ab3388

[17] Pang, J., Choi, K.-S.: Turbulent drag reduction by Lorentz force oscillation. Physics of Fluids **16**(5) (2004). https://doi.org/10.1063/1.1689711

[18] Breuer, K.S., Park, J., Henoch, C.: Actuation and control of a turbulent channel flow using lorentz forces. Physics of Fluids **16**(4), 897–907 (2004). https://doi.org/10.1063/1.1647142

[19] Mahfoze, O., Laizet, S.: Skin-friction drag reduction in a channel flow with streamwise-aligned plasma actuators. International Journal of Heat and Fluid Flow **66**, 83–94 (2017). https://doi.org/10.1016/J.IJHEATFLUIDFLOW.2017.05.013

[20] Quadrio, M., Ricco, P.: Initial response of a turbulent channel flow to spanwise oscillation of the walls. Journal of Turbulence **4** (2003). https://doi.org/10.1088/1468-5248/4/1/007

[21] Skote, M.: Comparison between spatial and temporal wall oscillations in turbulent boundary layer flows. Journal of Fluid Mechanics **730**, 273–294 (2013). https://doi.org/10.1017/jfm.2013.344

[22] Quadrio, M.: Drag reduction in turbulent boundary layers by in-plane wall motion. Philosophical Transactions of the Royal Society A: Mathematical, Physical and Engineering Sciences **369**, 1428–1442 (2011). https://doi.org/10.1098/RSTA.2010.0366

[23] Choi, K.S., DeBisschop, J.R., Clayton, B.R.: Turbulent boundary-layer control by means of spanwise-wall oscillation. https://doi.org/10.2514/2.526 **36**, 1157–1163 (2012). https://doi.org/10.2514/2.526

[24] Zong, H., Su, Z., Liang, H., Wu, Y.: Experimental investigation and reduced-order modeling of plasma jets in a turbulent boundary layer for skin-friction drag reduction. Physics of Fluids **34** (2022). https://doi.org/10.1063/5.0104609

[25] Straub, S., Vinuesa, R., Schlatter, P., Frohnapfel, B., Gatti, D.: Turbulent duct flow controlled with spanwise wall oscillations. Flow, Turbulence and Combustion **99**, 787–806 (2017). https://doi.org/10.1007/S10494-017-9846-6/FIGURES/14

[26] Güttler, A.: High accuracy determination of skin friction differences in an air channel flow based on pressure drop measurements. PhD thesis, Karlsruhe Institute of Technology (KIT) (2015). https://doi.org/10.5445/IR/1000048039

[27] Gatti, D., von Deyn, L.H., Forooghi, P., Frohnapfel, B.: Do riblets exhibit fully rough behaviour? Experiments in Fluids **61**, 81 (2020). https://doi.org/10.1007/s00348-020-2921-0

[28] von Deyn, L.H., Gatti, D., Frohnapfel, B.: From drag-reducing riblets to drag-increasing ridges. Journal of Fluid Mechanics **951**, 16 (2022). https://doi.org/10.1017/jfm.2022.796

[29] Astarita, T.: Analysis of interpolation schemes for image deformation methods in piv: Effect of noise on the accuracy and spatial resolution. Experiments in Fluids **40**, 977–987 (2006). https://doi.org/10.1007/S00348-006-0139-4

[30] Astarita, T.: Analysis of weighting windows for image deformation methods in piv. Experiments in Fluids **43**, 859–872 (2007). https://doi.org/10.1007/S00348-007-0314-2

[31] Astarita, T.: Analysis of velocity interpolation schemes for image deformation methods in piv. Experiments in Fluids **45**, 257–266 (2008). https://doi.org/10.1007/S00348-008-0475-7

[32] Kotsonis, M.: Diagnostics for characterisation of plasma actuators. Measurement Science and Technology **26**(9) (2015). https://doi.org/10.1088/0957-0233/26/9/092001

[33] Kriegseis, J., Simon, B., Grundmann, S.: Towards in-flight applications? a review on dielectric barrier discharge-based boundary-layer control. Applied Mechanics Reviews **68**(2) (2016). https://doi.org/10.1115/1.4033570

[34] Kriegseis, J., Grundmann, S., Tropea, C.: Airflow influence on the discharge performance of dielectric barrier discharge plasma actuators. Physics of Plasmas **19**(7) (2012). https://doi.org/10.1063/1.4736995

[35] Kriegseis, J., Barckmann, K., Frey, J., Tropea, C., Grundmann, S.: Competition between pressure effects and airflow influence for the performance of plasma actuators. Physics of Plasmas **21**(5) (2014). https://doi.org/10.1063/1.4880098

[36] Pereira, R., Kotsonis, M., De Oliveira, G., Ragni, D.: Analysis of local frequency response of flow to actuation: Application to the dielectric barrier discharge plasma actuator. Journal of Applied Physics **118**(15) (2015). https://doi.org/10.1063/1.4894518

[37] Kriegseis, J., Duchmann, A., Tropea, C., Grundmann, S.: On the classification of dielectric barrier discharge plasma actuators: A comprehensive performance evaluation study. Journal of Applied Physics **114**, 053301

(2013). https://doi.org/10.1063/1.4817366

[38] Choi, K.-S., Jukes, T., Whalley, R.: Turbulent boundary-layer control with plasma actuators. Philosophical Transactions of the Royal Society A: Mathematical, Physical and Engineering Sciences **369**(1940), 1443–1458 (2011). https://doi.org/10.1098/RSTA.2010.0362

[39] Serpieri, J., Hehner, M.T., Kriegseis, J.: Active electrode isolation for advanced plasma actuators. Sensors and Actuators A: Physical **343**, 113675 (2022). https://doi.org/10.1016/J.SNA.2022.113675

[40] Quadrio, M., Ricco, P., Viotti, C.: Streamwise-travelling waves of spanwise wall velocity for turbulent drag reduction. Journal of Fluid Mechanics **627**, 161–178 (2009). https://doi.org/10.1017/S0022112009006077